SUPPLEMENTARY INFORMATION

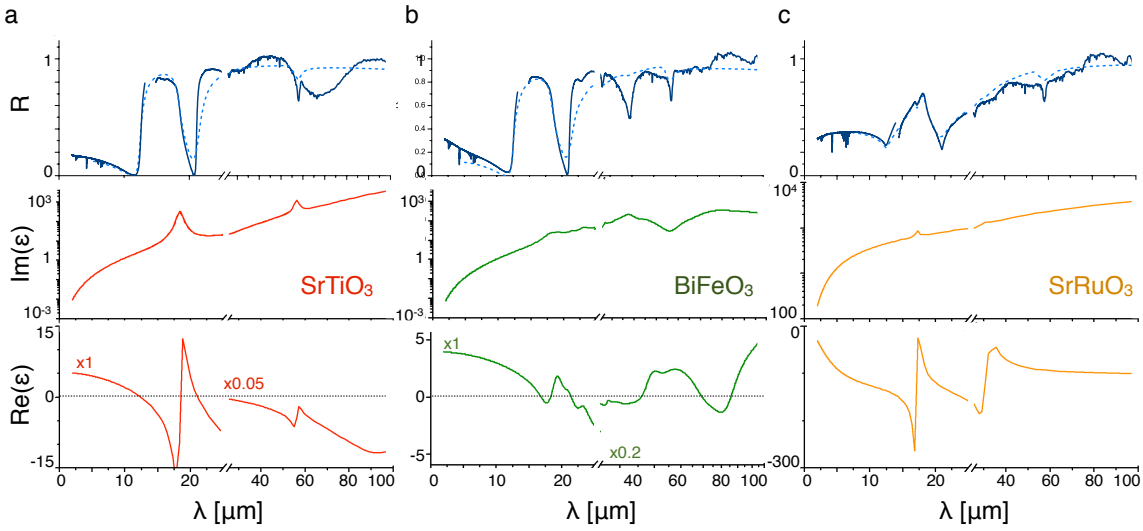

SUPPLEMENTARY FIGURE S 1. **FTIR spectra and dielectric constants of perovskites.** We compare the dielectric constants of all constituents of the perovskite-based superlens with Fourier transform infrared (FTIR) reflection spectra. We find a good agreement between literature [20, 21] and the spectra of $SrTiO_3$ and $BiFeO_3$. For $SrRuO_3$, we found no literature data for the wavelength range of our interest and determined the dielectric constant from the FTIR spectra. (a) Strontrium titanate ($SrTiO_3$): FTIR spectra (blue solid line) on 1 mm thick substrate and fit of spectra (dashed curve) by the depicted permittivity values from Spitzer et al. [20]. (b) Bismuth ferrite ($BiFeO_3$): FTIR spectra (blue solid line) on 195 nm thick $BiFeO_3$ on 1 mm thick $SrTiO_3$ substrate and fit of spectra (dashed curve) by the depicted permittivity values from Kamba et al. [21]. (c) Strontrium ruthenate ($SrRuO_3$): FTIR spectra (blue solid line) on 10 nm thick $SrRuO_3$ on 1 mm thick $SrTiO_3$ substrate and fit of spectra (dashed curve) leads to the depicted permittivity values. All fits were calculated using Reffit software by Kuzmenko, University of Geneva, designed for fitting optical spectra with various physical models (http://optics.unige.ch/alexey/reffit.html).

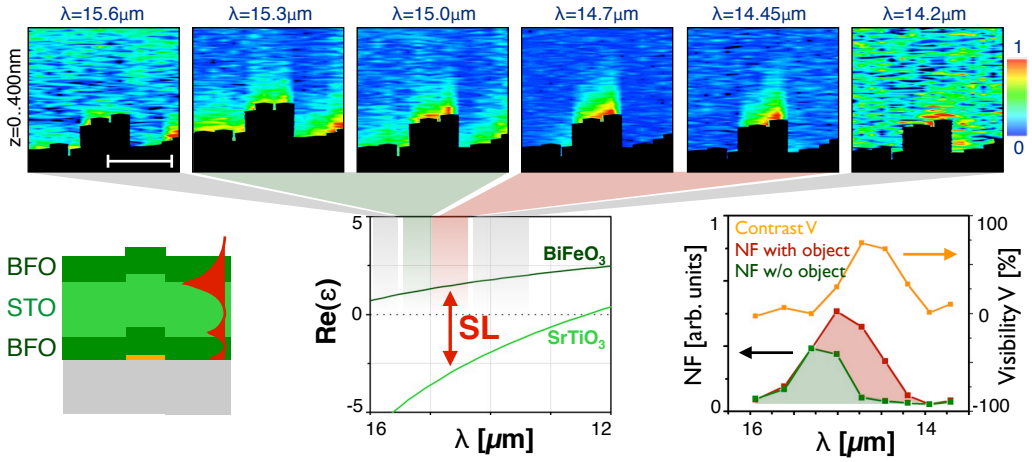

SUPPLEMENTARY FIGURE S 2. **Normalized cross sections on a symmetric superlens.** Measured near-field signal as a function of the distance and the sample position for selected wavelengths. The topography of the sample and the position of the $SrRuO_3$ object is reflected by the dark areas at the bottom of the figures (horizontal range: 12 μm, scalebar is 6 μm). The lower panel displays (from left to right): a sketch of the studied system, real parts of the dielectric constants of the layer materials, and the spectral behavior of near-field signals with and without objects as well as the corresponding contrast V calculated from this data. The marked areas correspond to an observation of no signal (grey), phonon-enhance near-field signals (green), and enhanced evanescent fields due to the superlensing effect (red). We observe no signal on the sample surface for $\lambda < 14.2$ μm and $\lambda > 15.6$ μm except for some scattering effects. Around the superlensing wavelength, at $\lambda = 14.8$ to 14.4 μm, polaritons at both interfaces of layer B are strongly coupled and the object appears brighter than the surrounding areas. In contrast to the asymmetric lens, the maximum of the superlensed signal is located at the sample surface for all wavelengths. The reason lies in the additional spacer layer of $BiFeO_3$ with a thickness of 200 nm. Due to this layer, the probe can not approach the $SrTiO_3$ interface close enough to observe the intriguing maximum which we discussed in Fig. 5 of the main manuscript for the asymmetric lens.

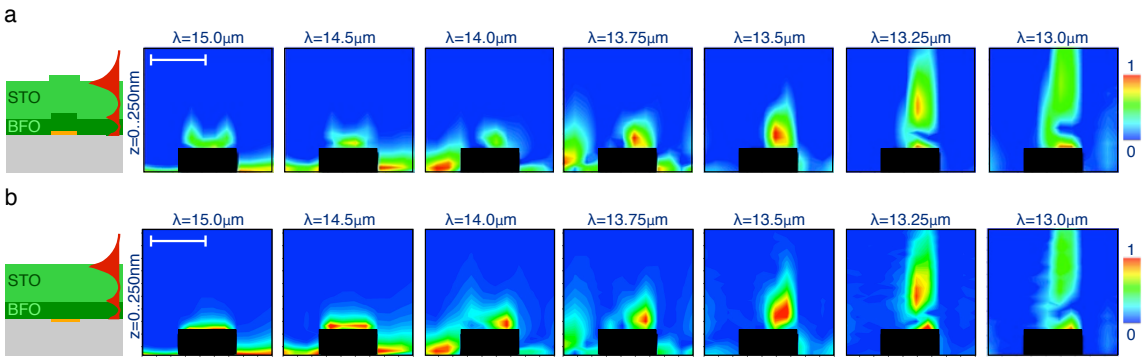

SUPPLEMENTARY FIGURE S 3. **Simulated cross sections with and without protrusion.** (a) with protrusion (same data as depicted in Fig. 5), (b) without protrusion i.e. with ideally flat interfaces. In both (a) and (b), the horizontal range is 12 μm and the scalebar is 6 μm. Please note that for the simulations without protrusions, we elevated the data by inserting a box at the position of the $SrRuO_3$ object for an easier comparison. In both simulations we observe the same behavior of the signal in the spectral response as well as its lateral and vertical distribution, confirming that the probe-object coupling and our experimental results are not correlated with the topographic step (please note that the protrusion of about 50 nm is very small compared to the wavelength of about $\lambda = 13$ μm to 16 μm and the smallest object size of 3 μm). However, the effect of localized edge modes for $\lambda > 14.0$ μm as discussed in the main manuscript does not appear for flat interfaces (b).

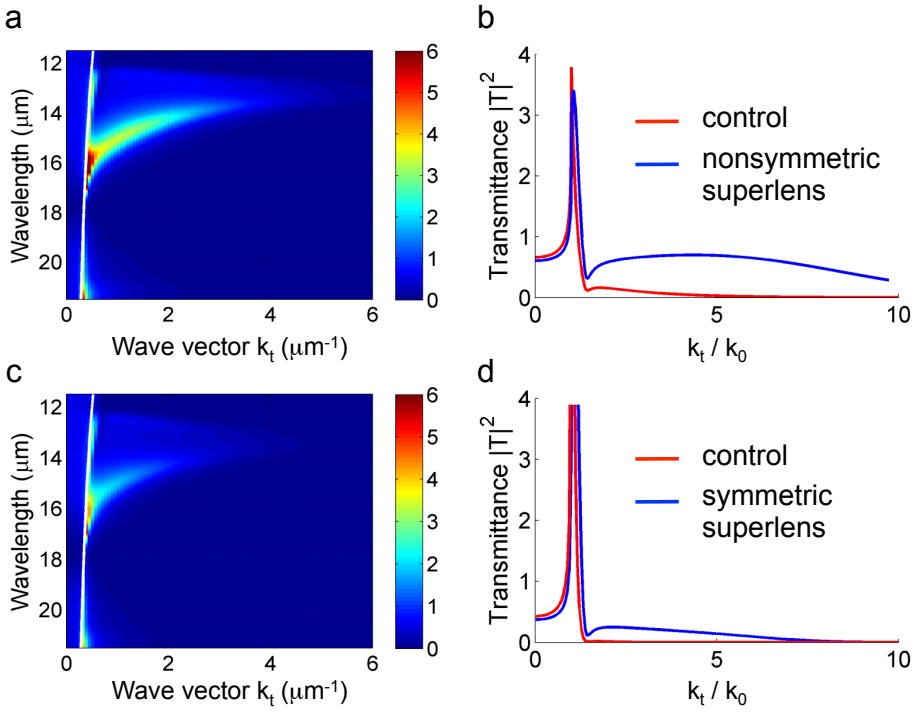

SUPPLEMENTARY FIGURE S 4. **Transfer function of the asymmetric and symmetric superlens.** (a) The isothermal contour of transfer function for asymmetric superlens in the wavelength range of our interest. The color represents the transfer function. The white curve represents the light line in air. (b) The transfer functions for asymmetric superlens and the control sample at 13.5 μm wavelength. The control sample replaces the 400 nm $SrTiO_3$ film in the superlens by a 400 nm $BiFeO_3$ layer. Clearly, evanescent waves are enhanced by the superlens over a large range of wave vector of up to 10 k_0. The sharp peaks are due to total internal reflection. (c) and (d) are similar to (a) and (b), respectively, but for a symmetric superlens and the corresponding control sample. The dispersion curves of the two types of superlenses are similar, in particular they both converge around 13.5 μm. However, the actual performance of the symmetric superlens is not as good as the asymmetric case in terms of the field enhancement and wave vector bandwidth, because of the additional 200 nm $BiFeO_3$ layer on top of the $SrTiO_3$ film.